Turbulence intensities in large-eddy simulation of wall-bounded flows

H. J. Bae,[1,2,*] A. Lozano-Durán,[1] S. T. Bose,[2,3] and P. Moin[1]
[1]*Center for Turbulence Research, Stanford University, Stanford, California 94305, USA*
[2]*Institute for Computation and Mathematical Engineering, Stanford University, Stanford, California 94305, USA*
[3]*Cascade Technologies, Inc., Palo Alto, California 94303, USA*

(Received 24 July 2017; published 22 January 2018)

A persistent problem in wall-bounded large-eddy simulations (LES) with Dirichlet no-slip boundary conditions is that the near-wall streamwise velocity fluctuations are overpredicted, while those in the wall-normal and spanwise directions are underpredicted. The problem may become particularly pronounced when the near-wall region is underresolved. The prediction of the fluctuations is known to improve for wall-modeled LES, where the no-slip boundary condition at the wall is typically replaced by Neumann and no-transpiration conditions for the wall-parallel and wall-normal velocities, respectively. However, the turbulence intensity peaks are sensitive to the grid resolution and the prediction may degrade when the grid is refined. In the present study, a physical explanation of this phenomena is offered in terms of the behavior of the near-wall streaks. We also show that further improvements are achieved by introducing a Robin (slip) boundary condition with transpiration instead of the Neumann condition. By using a slip condition, the inner energy production peak is damped, and the blocking effect of the wall is relaxed such that the splatting of eddies at the wall is mitigated. As a consequence, the slip boundary condition provides an accurate and consistent prediction of the turbulence intensities regardless of the near-wall resolution.

DOI: 10.1103/PhysRevFluids.3.014610

I. INTRODUCTION

Accurate prediction of turbulence intensities is of great importance in both external and internal flows. In the former, they are directly related to the noise signature around airframe components [1,2]. In particle laden flows, turbulence intensities are important for prediction of particle trajectories in the vicinity of the walls and hence to capture correctly the turbophoretic effect [3,4]. Despite its relevance, it has been observed in large-eddy simulations (LES) that the near-wall streamwise velocity fluctuations are overpredicted, while those in the wall-normal and spanwise directions are underpredicted. The problem is particularly aggravated when the near-wall region is not well resolved and is usually alleviated by refining the grid [5,6]. However, the near-wall resolution requirements to accurately compute the boundary layer are estimated to scale as $\mathrm{Re}^{9/5}$, where Re is the characteristic Reynolds number of the problem [7]. A more recent study by Choi and Moin [8] using more accurate correlations for the skin friction coefficients concluded that the cost is $\sim\mathrm{Re}^{13/7}$, which is still far too expensive for many practical problems despite the improvement compared to the $\mathrm{Re}^{37/14}$ scaling required for direct numerical simulation (DNS).

Some recent works to improve the prediction of first-order statistics in coarse LES are based on the Reynolds-averaged Navier-Stokes (RANS) equations, such as the constrained LES [9] and explicit algebraic models [6], among others. However, these approaches rely on empirical parameters,

*hjbae@stanford.edu

which may be not applicable across different flow configurations. Other works, such as the integral length-scale approximation models [10], have focused on modifying the LES eddy viscosity model with moderate improvements on first-order statistics. These approaches reduce substantially the grid resolution requirements, although the cost is still expected to scale as $\mathrm{Re}^{13/7}$.

Another approach is to fully model the near-wall flow such that only the large-scale motions in the outer region of the boundary layer are resolved. In this case, the grid point requirements for wall-modeled LES scale at most linearly with the Reynolds number [8]. Several strategies for modeling the near-wall region have been explored in the past, and most of them are effectively applied by replacing the no-slip boundary condition in the wall-parallel directions by a Neumann condition. This is motivated by the observation that with the no-slip condition, most subgrid scale models do not provide the correct stress at the wall when the near-wall layer is not resolved by the grid [11]. When the no-slip condition is replaced by the Neumann boundary condition, the prediction of the near-wall velocity fluctuations is known to improve considerably, although this has been observed only for near-wall resolutions coarse enough to avoid the near-wall region where turbulence intensity peaks [12–15]. No physical explanation of the mechanisms involved has been provided yet. In canonical flows, the first grid point can be chosen to bypass the near wall peaks. However, this requires *a priori* knowledge of the local Reynolds number, which is not always available for arbitrary flow configurations. The problem becomes particularly relevant when dealing with flows over geometrically complex surfaces, where the resolution to avoid the turbulence intensity peaks near the wall is unknown.

Examples of the most popular and well-known wall models using the Neumann boundary condition are the traditional wall-stress models (or approximate boundary conditions), where the wall stress is computed using either the law of the wall [16–18], the solution obtained by solving a simplified version of the boundary layer equations close to the wall, or the RANS equations [12,14,19,20]. The reader is referred to [21–24] for a more comprehensive review of wall-modeled LES. In all of the wall models presented above, the no-transpiration condition was still maintained in the wall-normal velocity, and only recently this has been replaced by a transpiration boundary condition as in Ref. [25].

In the present study, we investigate the physical mechanisms behind the improved prediction of the near-wall velocity fluctuations in an LES of turbulent channel flow. For this purpose, we analyze three different boundary conditions, i.e., Dirichlet no-slip, Neumann with no transpiration (traditional wall models), and Robin boundary condition (slip boundary condition with transpiration). A physical explanation of the improvements are given in terms of the streak breakup and the suppression of spurious splat [26] formation when transpiration is allowed.

The paper is organized as follows. In Sec. II, we introduce the boundary conditions used and describe the numerical experiments in our analysis. In Sec. III, we study the physical mechanisms involved in the prediction of the near-wall velocity fluctuations. Finally, a summary and conclusions are offered in Sec. IV.

II. NUMERICAL SETUP

A. Boundary conditions

We describe the three different boundary conditions used in the present work for a channel flow configuration. The Dirichlet no-slip boundary condition is defined as $\bar{u}_i|_w = 0$, where the indices $i = 1,2,3$ denote the three spatial directions represented by x_1, x_2, and x_3, which are the streamwise, wall-normal, and spanwise directions, respectively. The flow velocities are denoted by u_i, $\bar{(\cdot)}$ represents the resolved field in LES, and $(\cdot)|_w$ indicates quantities evaluated at the wall. The Neumann boundary condition without transpiration is defined as

$$\frac{\partial \bar{u}_1}{\partial n} = \alpha, \quad \bar{u}_2 = 0, \quad \frac{\partial \bar{u}_3}{\partial n} = 0, \tag{1}$$

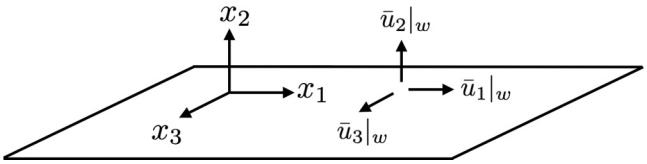

FIG. 1. Sketch of the slip boundary condition with transpiration ($\bar{u}_2|_w \neq 0$) for a flat wall.

where n is the wall-normal direction and α is a prescribed value described in Sec. II B.

We define the slip boundary condition with transpiration as

$$\bar{u}_i|_w = l_i \left.\frac{\partial \bar{u}_i}{\partial n}\right|_w + v_i, \quad i = 1,2,3, \tag{2}$$

where repeated indices do not imply summation. We define l_i to be the slip lengths and v_i the slip velocities. In general, both the slip lengths and velocities are functions of space and time. A slip boundary condition similar to Eq. (2) has been used by Bose and Moin [25] in the context of wall-modeled LES, together with a dynamic procedure for determination of the local slip length free of any *a priori* specified coefficients. A sketch of the slip boundary condition for a flat wall is given in Fig. 1.

It should be noted that the choice of l_i and v_i must comply with the symmetries of the flow and the impermeability constraint of the wall on average. In particular, for a channel flow configuration, the slip boundary condition should satisfy

$$\langle \bar{u}_i \rangle|_w = \left\langle l_i \left.\frac{\partial \bar{u}_i}{\partial x_2}\right|_w \right\rangle + \langle v_i \rangle = 0, \quad i = 2,3, \tag{3}$$

where $\langle \cdot \rangle$ denotes average in homogeneous directions and time. In the present study, we will consider l_i constants and $v_i = 0$ for $i = 1,2,3$. These constraints are consistent with Eq. (3), since $\langle \bar{u}_i \rangle|_w = 0$ and $\langle \partial \bar{u}_i / \partial x_2 \rangle|_w = 0$ for $i = 2,3$. We have set $v_1 = 0$ without loss of generality, since its average effect can be absorbed by moving the frame of reference at constant uniform velocity. Then, a consistent slip boundary condition for the channel can be written as

$$\bar{u}_i|_w = l_i \left.\frac{\partial \bar{u}_i}{\partial x_2}\right|_w, \tag{4}$$

which is the form used in the remainder of the paper.

B. Numerical experiments

We perform a set of plane turbulent channel LESs. The simulations are computed with a staggered second-order finite difference [27] and a fractional-step method [28] with a third-order Runge-Kutta time-advancing scheme [29]. The dynamic Smagorinsky model is used as the subgrid scale model [30,31]. Periodic boundary conditions are imposed in the streamwise and spanwise directions. The size of the channel is $2\pi\delta \times 2\delta \times \pi\delta$ in the streamwise, wall-normal, and spanwise directions, respectively, where δ is the channel half-height. It has been shown that this domain size is large enough to accurately predict one-point turbulence statistics for friction Reynolds number Re_τ up to 4200 [32]. The grid resolutions for this set of cases are chosen to be comparable to those found in the literature [5].

At the wall, three different boundary conditions as described in Sec. II A are applied: the no-slip boundary condition, the Neumann boundary condition without transpiration, and the slip boundary condition with transpiration. The channel was driven by imposing a constant mean pressure gradient and all cases were run for at least $100\delta/u_\tau$ after transients, where u_τ is the friction velocity. For the Neumann condition, α in Eq. (1) was adjusted to match the target Re_τ at each time step. The same was done for the slip case by modifying the slip lengths (see [33] for details). We have adopted the

TABLE I. Tabulated list of cases. The case name is given in the first column, where the first two uppercase letters indicate the boundary condition used: no-slip (NS), Neumann (NE), and slip (SL). The middle number is Re_τ for $\mathrm{Re}_\tau = 550, 2000$. The lowercase letter is used to denote the stretching of the grid: stretched (s) and uniform (u). The last number indicates $N_{1,2,3}$, the number of grid points which are the same in all three directions. Here Δ_2 is the wall-normal grid size at the wall. The relative intensity of the peaks for u_1' at $x_2^{\max}$ for LES with respect to DNS is given in the sixth column. The value of $x_2^{\max}$ is the maximum of $x_2^{\max,\mathrm{LES}}$ and $x_2^{\max,\mathrm{DNS}}$, where $x_2^{\max,\mathrm{LES/DNS}}$ is the location of maximum value of u_1' for LES and DNS, respectively. The symbols for each case are used in the subsequent plots.

Case	Re_τ	$N_{1,2,3}$	Δ_2^+	Δ_2/δ	$\frac{\langle u_1'^2(x_2^{\max})\rangle^{1/2}}{\langle u_{1\mathrm{DNS}}'^2(x_2^{\max})\rangle^{1/2}}$	Symbols
NS550s32	550	32	1.41	2.6×10^{-3}	1.75	× (blue)
NS550s64	550	64	0.64	1.2×10^{-3}	1.24	▽ (green)
NS2000s64	2000	64	2.35	1.2×10^{-3}	1.90	◯ (red)
NS550u32	550	32	34.2	6.25×10^{-2}	1.07	□ (green)
NE550u32	550	32	34.2	6.25×10^{-2}	1.15	△ (magenta)
SL550u32	550	32	34.2	6.25×10^{-2}	1.00	+ (red)

simplification of imposing the correct mean component of the wall stress, which has been shown by Lee *et al.* [13] to be sufficient for prediction of low-order turbulence statistics in channel flow for the Neumann boundary condition. We have also performed a similar test for the slip boundary condition as a function of time, and the resulting statistics are similar to the ones obtained using a constant mean wall stress.

The details of the simulations are given in Table I. The table is divided in two blocks. The first block is used to assess whether the problem under investigation scales in inner or outer units. The second block serves to evaluate the effect of different boundary conditions. The results are compared with DNS data at the corresponding Reynolds number from Del Álamo *et al.* [34] and Hoyas and Jiménez [35].

III. RESULTS AND DISCUSSION

A. Scaling of the problem

An example of the over- and underestimation of the turbulence intensities is shown in Figs. 2(a) and 2(b). The relative intensity of the peaks for u_1' with respect to DNS is given in Table I, where $(\cdot)'$ denotes the root-mean-square (rms) of the fluctuations.

The first question is to assess whether the grid requirements to address this problem scales in outer or inner units for no-slip LES. As demonstrated in Fig. 2(a), the resolution used in the case NS550s32 ($\mathrm{Re}_\tau = 550$) results in large peaks for the streamwise rms velocity fluctuations, whereas doubling the number of grid points in each direction (NS550s64) improves the prediction noticeably [Fig. 2(c)]. The result worsens again by increasing the Reynolds number from $\mathrm{Re}_\tau = 550$ to 2000 while maintaining the finer grid resolution [NS2000s64, Fig. 2(d)]. This suggests that, for the no-slip boundary condition, the problem is independent of the outer-layer eddies and the required near-wall grid to avoid under- or overpredictions scales in wall units.

B. Effect of the streak breakup

The cause of the problem is analyzed in Figs. 3 and 4, which show instantaneous snapshots and the autocorrelations of u_1' at $x_2^+ \approx 15$ for a selection of the cases from Table I. The results reveal that when the peaks are not well predicted (case NS550s32), as in Figs. 3(a) and 4(a), the associated flow is dominated by streamwise streaks several times longer than those of the DNSs. This is consistent with observations in Refs. [6,36,37]. On the other hand, the lengths of the streaks developed in the flow when increasing the resolution [case NS550s64, Fig. 4(b)] or introducing the slip boundary condition [case SL550u32, Figs. 3(b) and 4(c)] are comparable to those from DNSs. Although not

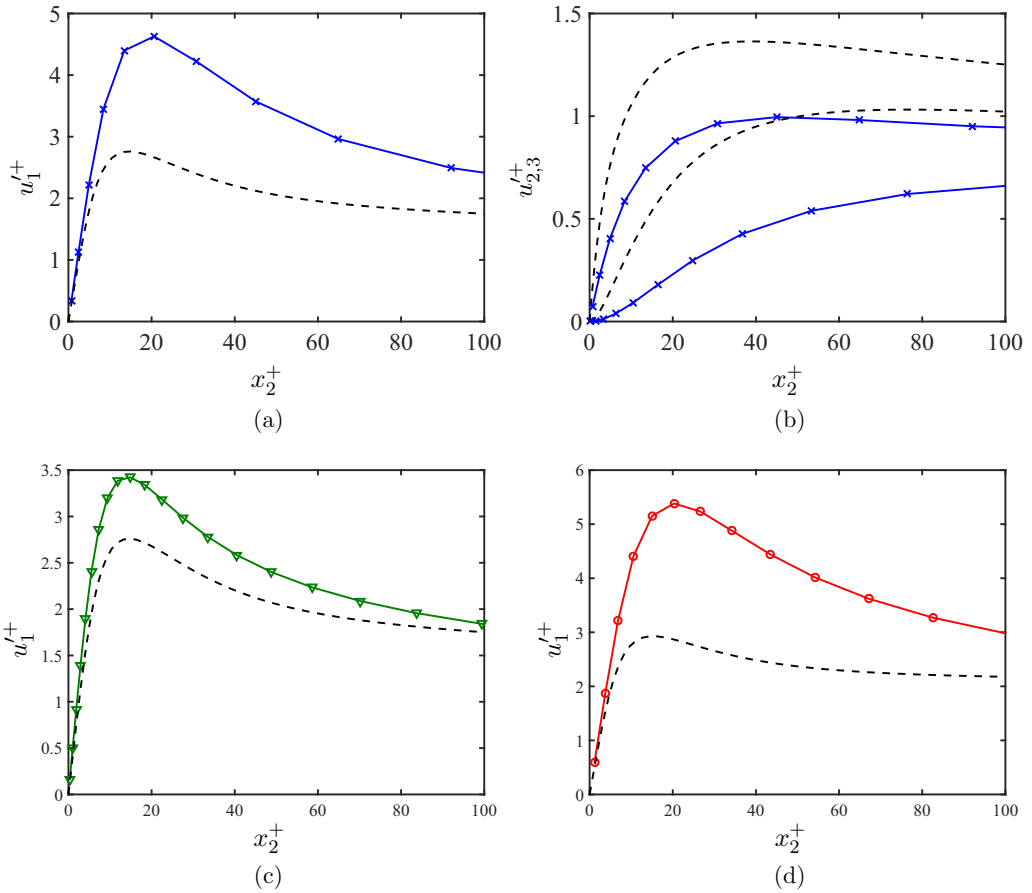

FIG. 2. The rms velocity fluctuations for NS550s32 in the (a) streamwise and (b) spanwise (top) and wall-normal (bottom) directions. Also shown are the streamwise rms velocity fluctuations for (c) NS550s64 and (d) NS2000s64. The symbols are as in Table I. Dashed lines are DNS data at the corresponding Reynolds number.

shown, the Neumann boundary condition (NE550u32) yields results similar to those observed for the slip case. Note that the improvement achieved with the Neumann or slip boundary condition does not increase the computational cost of the simulation since grid refinement was not required, in contrast to the improvements attained using the no-slip boundary condition in Fig. 2(c).

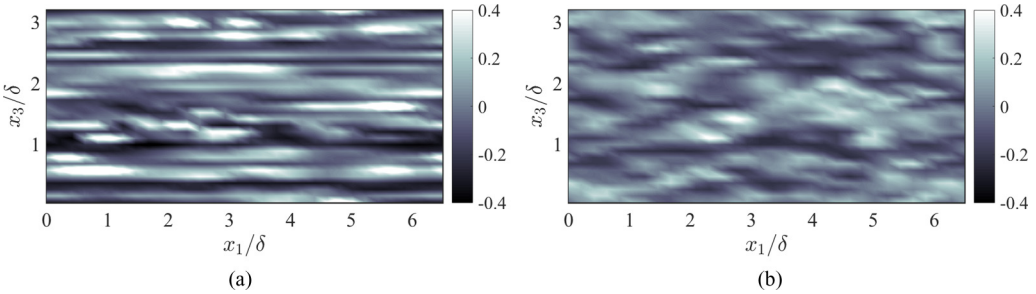

FIG. 3. Instantaneous snapshots of the streamwise velocity component at $x_2^+ \approx 15$ for (a) NS550s32 and (b) SL550u32.

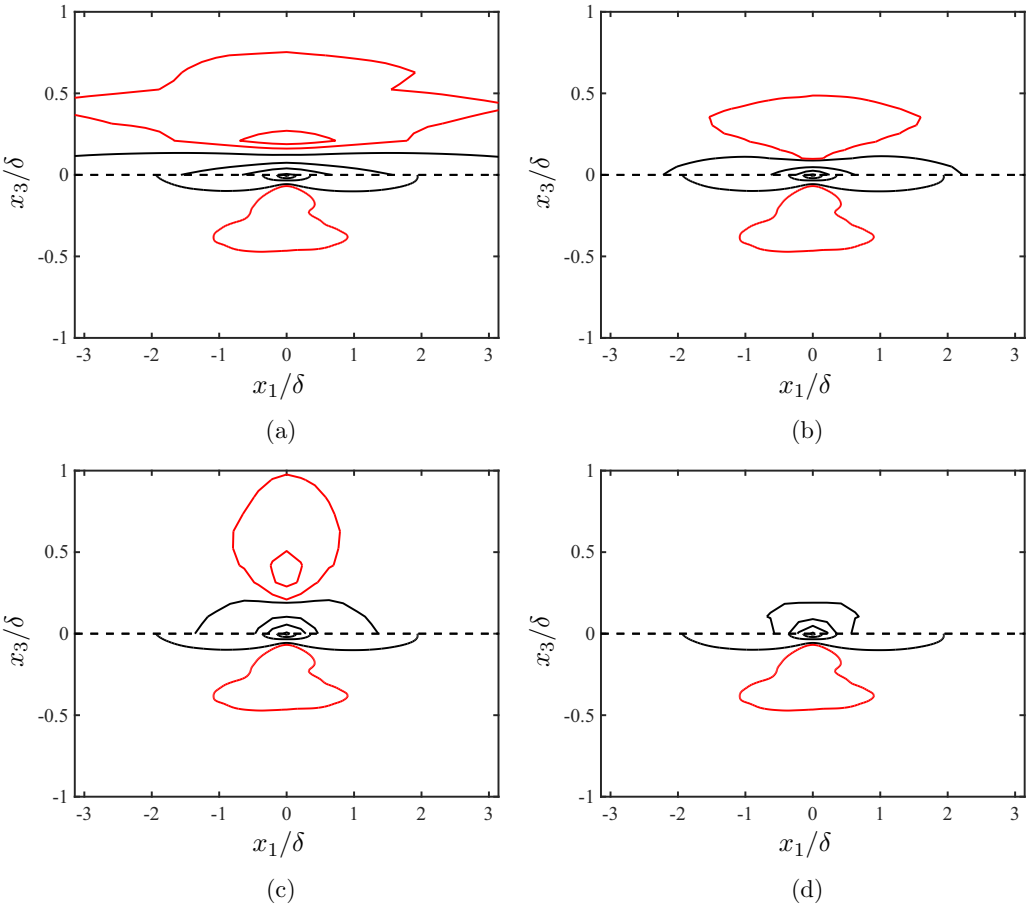

FIG. 4. Autocorrelations of the streamwise velocity component at $x_2^+ \approx 15$ for (a) NS550s32, (b) NS550s64, (c) SL550u32, and (d) NS550u32. The upper half of the autocorrelation is for LES and the lower half for DNS. Contour lines are for positive correlations of 5% and 35% of the maximum (black) and negative correlations of 2% and 7% of the maximum (red).

The interpretation from the previous results is that, in the case of no-slip, the near-wall dynamics are altered in such a way that the streaks are unable to follow their natural cycle of meandering and breakup [38,39], which manifests itself in the flow by a strong u_1' and reduced u_2' and u_3'. Other investigations on drag reduction have reported a similar behavior in the turbulence intensities by controlling the near-wall streaks [40] or by adding a stochastic forcing term to break up the large-scale structures [41,42].

The previous interpretation is further supported by the improved intensities (Fig. 5) and shorter streamwise streaks [Fig. 4(d)] in the case NS550u32, where the first interior grid point is such that the streaks below $x_2^+ \approx 15$ are bypassed while maintaining the no-slip boundary condition. A more systematic analysis of the effect of the first grid point is shown in Fig. 6(a), where the grid is stretched in order to modify Δx_2 at the wall. For coarse resolutions with $\Delta x_2^+ > 15$, the overprediction of u_1' is mitigated for all boundary conditions. By stretching the grid such that Δx_2 is finer at the wall, only the slip boundary condition provides good predictions of the streamwise turbulence intensities regardless of the grid resolution, whereas the results from the no-slip and Neumann boundary conditions degrade for $\Delta x_2^+ < 15$. As an example, the streamwise rms velocities for the most stretched grid are shown in Fig. 6(b). Note that despite the good prediction of the no-slip case for resolutions with $\Delta x_2^+ > 15$, this is not a practical solution as the no-slip condition cannot be used in context of wall-modeled

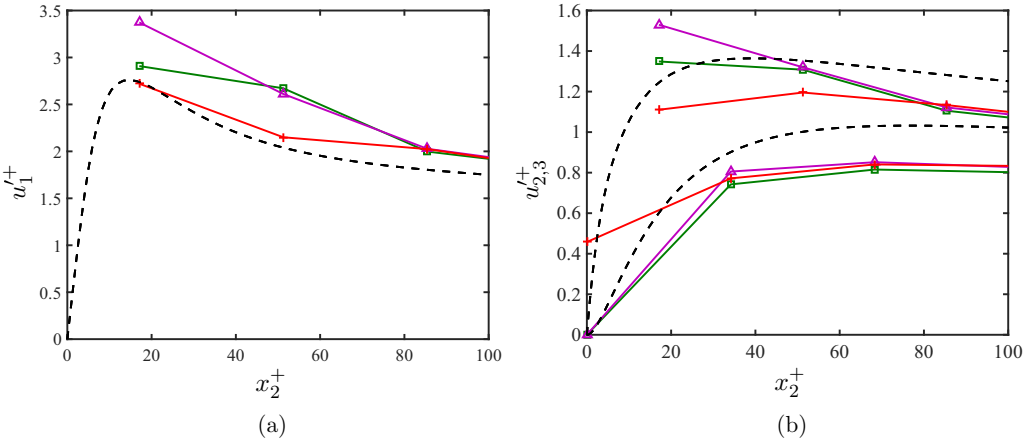

FIG. 5. The rms (a) streamwise and (b) spanwise (top) and wall-normal (bottom) velocity fluctuations for cases NS550u32, NE550u32, and SL550u32. Symbols as in Table I. Dashed line is DNS.

LES. Another important remark is that in most wall-modeled LES, the Neumann boundary condition has been used on canonical flows such as channel or boundary layer flows, where the near-wall grid resolution is usually chosen to satisfy $\Delta x_2^+ > 15$. Our analysis is relevant for those flow configurations where the local Reynolds number is not known *a priori* and hence the first grid point may lie in the region $\Delta x_2^+ < 15$. Finally, the results in Fig. 6(a) highlight the fact that providing the perfect wall model (correct mean wall stress) is not enough for good prediction of the turbulence intensities at all resolutions and the intensities also depend on the form of the boundary condition.

According to the previous results, both Neumann and slip boundary conditions improve the prediction of the turbulence intensities by avoiding the formation of long streaks; however, the mechanisms involved are different for each case. To analyze in more detail these mechanisms, the production $\mathcal{P}$, pressure strain Π, and turbulent diffusion $\mathcal{T}$ components of the streamwise turbulence intensity budget are plotted in Figs. 7(a)–7(c). The choice of these quantities is motivated by the fact that the energy source for $u_1'^2$ is given by the production term, while the transfer of energy to the $u_2'^2$ and

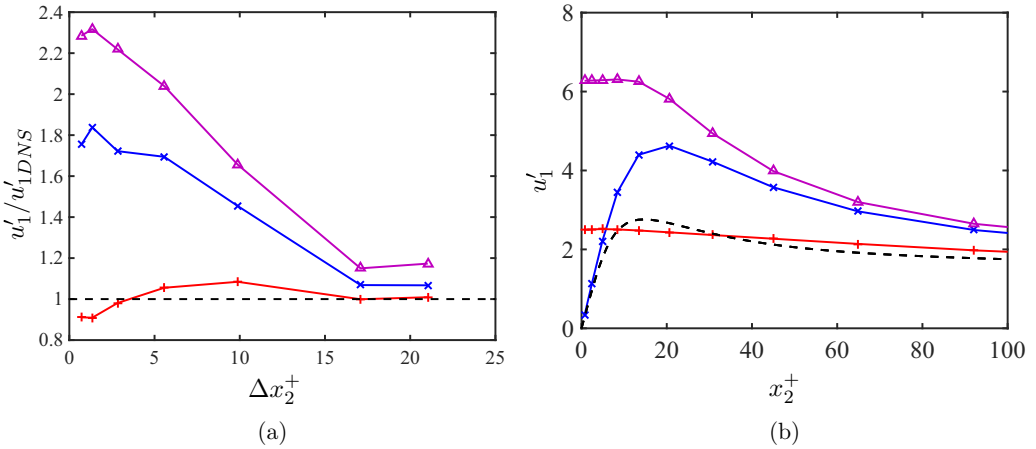

FIG. 6. (a) Relative intensity of the peaks at $x_2^{\max}$ for u_1' with respect to DNS as a function of Δx_2 at the wall, where $x_2^{\max}$ is as defined in Table I. (b) Streamwise rms velocities for the most stretched mesh with $\Delta x_2^+ = 1.41$. Symbols are no-slip, $\times$ (blue); Neumann, $\triangle$ (magenta); and slip, $+$ (red) boundary conditions.

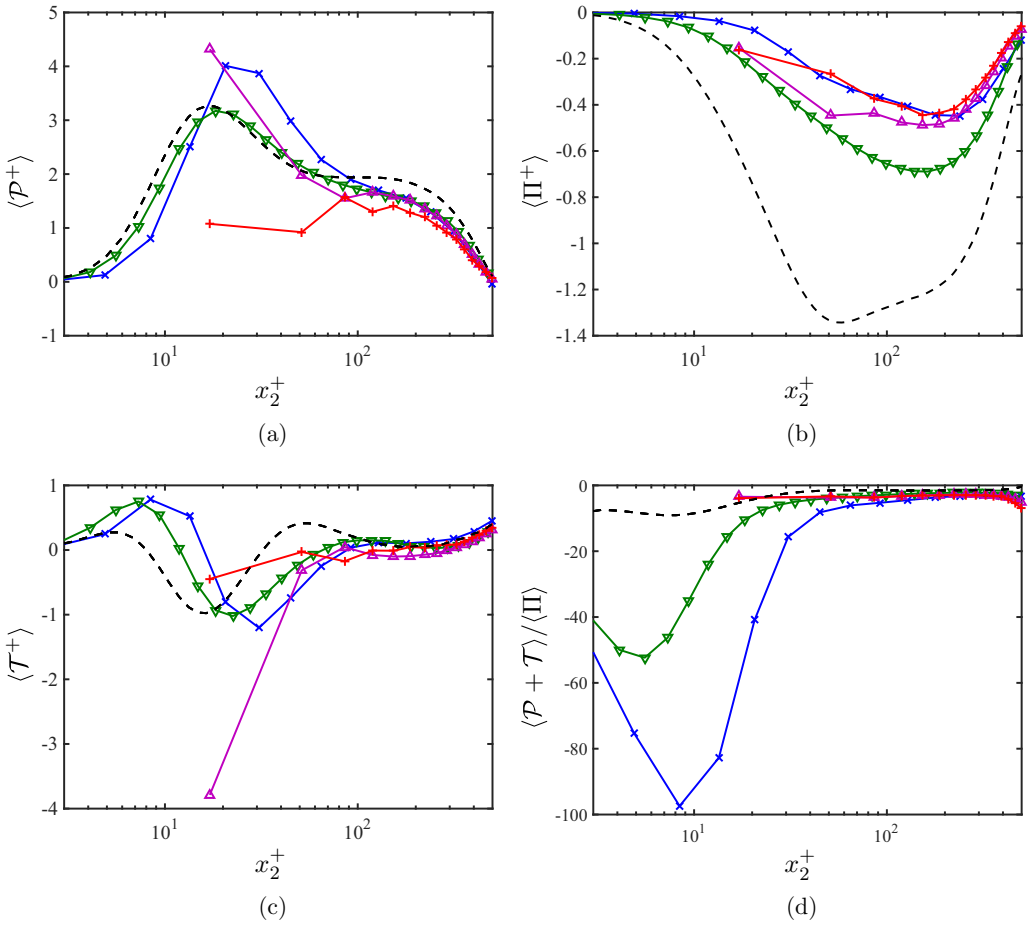

FIG. 7. (a) Average production $\langle \mathcal{P} \rangle$, (b) pressure strain $\langle \Pi \rangle$, and (c) turbulent diffusion $\langle \mathcal{T} \rangle$ for the streamwise turbulence intensity budget and (d) $\langle \mathcal{P} + \mathcal{T} \rangle / \langle \Pi \rangle$ for NS550s32, NS550s64, NE550u32, and SL550u32. Symbols are as in Table I. The dashed line is DNS.

$u_3'^2$ components is provided through the streamwise pressure-strain correlation [43]. The turbulent diffusion term is also included since it is used to explain the improvements with the Neumann boundary condition at coarse near-wall grid resolutions.

In all cases, the magnitude of the pressure strain is underestimated, and moderate improvements appear by refining the grid or using either the Neumann or slip boundary condition. Regarding the production, the no-slip cases are characterized by a strong near-wall peak. On the contrary, this peak is absent for cases with slip, where most of the production is concentrated far from the wall. Similar results are observed for all slip cases shown in Fig. 6(a). In the case of the Neumann boundary condition, the strong near-wall maximum in the production term is still present but is compensated by the turbulent diffusion term, which transports the excess energy away from the wall. This is only the case when the near-wall resolution bypasses the near-wall peaks. For Neumann cases with $\Delta x_2^+ < 15$ in Fig. 6(a), the magnitude of the turbulent diffusion term is reduced near the wall, while the strong peak in the production term persists (not shown).

The above results are consistent with the streak lengths observed in Fig. 4 and it could be hypothesized that the excess of $\mathcal{P} + \mathcal{T}$ intensifies the streaks (stronger u_1') while the lack of pressure strain reduces the distribution of the energy to the other two velocity components (weaker u_2' and u_3'). This is further supported by the results in Fig. 7(d), which shows that the ratio $\langle \mathcal{P} + \mathcal{T} \rangle / \langle \Pi \rangle$

approaches the DNS value for those cases where the under- and overshoots of the rms velocity fluctuations are less pronounced.

C. Wall blocking effect

An additional cause of the problem may be attributed to the formation of splats due to the blocking effect of the wall. Splats are local regions of stagnation point flow resulting from fluid impinging on a wall and have been investigated in Ref. [26]. Here we study the effect of the splats on the turbulence intensities by comparing the cases NE550u32 (Neumann boundary condition with no transpiration) and SL550u32 (slip boundary condition with transpiration). The resulting rms velocity fluctuations are plotted in Fig. 5. Note that $\bar{u}_2'$ is not zero at the wall for the slip case due to transpiration. Although not shown, for coarser grid resolutions, the required slip lengths to match the target Re_τ are larger, which leads to a larger variability in the transpiration velocities as well. As the grid is refined, the slip length (and hence $\bar{u}_2'$) approaches zero. The results in Fig. 5 show that the blocking effect of the wall intensifies the splats, increasing the wall-parallel turbulence intensities (u_1' and u_3') near the wall. Compared to the traditional Neumann condition, better predictions of the streamwise velocity fluctuations are obtained when transpiration is allowed due to the local nonzero $\bar{u}_2$ which reduces the formation of splats.

IV. CONCLUSION

In this study, we have investigated the classic over- and underprediction of the rms velocity fluctuations close to the wall, which has been a persistent problem for LES with poor near-wall resolution. We have performed a set of LESs of turbulent channel flow in order to provide a physical explanation in terms of streak breakup and splat formation near the wall.

We have shown that in LES with no-slip boundary condition at the wall, the problem of over- or underprediction of turbulence intensities is independent of the the outer layer dynamics. The required near-wall resolution scales in wall units, making the no-slip boundary condition impractical at high Reynolds numbers. Wall-modeled LES is the most feasible approach compared to wall-resolved LES or DNS, as the required grid resolution scales at most linearly with Reynolds number. In wall-modeled LES, the no-slip boundary condition is typically replaced by a Neumann condition without transpiration, which is known to alleviate the problem when the near-wall resolution is such that the near-wall peaks are not resolved. We have shown that further improvements can be obtained by using a slip boundary condition with transpiration. Furthermore, contrary to the Neumann boundary condition, the prediction of the turbulence intensities is independent of the near-wall resolution. This is advantageous in flows over complex geometries, where the local Reynolds number of the flow is not known and the grid resolution cannot be judiciously chosen *a priori*. The consistent prediction of the slip boundary condition also provides a more monotonic convergence towards the DNS solution with grid refinement.

Our investigation reveals that the reason for the inaccurate predictions of the turbulence intensities can be traced back to the inability of the streaks to follow the natural dynamic cycle of meandering and breakup, which results in stronger streamwise fluctuations and weaker crossflow intensities. The Neumann boundary condition (for coarse near-wall grid resolutions) and the slip condition (for all grid resolutions investigated) avoid the energy pileup in u_1' by reducing the production of streamwise turbulence intensity, which in turn compensates for the underestimated redistribution of energy to u_2' and u_3'. As a consequence, the ratio $\langle \mathcal{P} + \mathcal{T} \rangle / \langle \Pi \rangle$ becomes closer to the DNS value for those cases with improved predictions. Further improvements are obtained by using the slip with transpiration and can be attributed to the suppression of splats by relaxing the blocking effect of the wall.

ACKNOWLEDGMENT

This work was supported by NASA under the Transformative Aeronautics Concepts Program (Grant No. UNIX15AU93A).

[1] M. M. Choudhari and M. R. Khorrami, Effect of three-dimensional shear-layer structures on slat cove unsteadiness, AIAA J. **45**, 2174 (2007).
[2] Y. Zhang, H. Chen, K. Wang, and M. Wang, Aeroacoustic prediction of a multi-element airfoil using wall-modeled large-eddy simulation, AIAA J. **55**, 4219 (2017).
[3] S. Balachandar and J. K. Eaton, Turbulent dispersed multiphase flow, Annu. Rev. Fluid Mech. **42**, 111 (2010).
[4] M. Caporaloni, F. Tampieri, F. Trombetti, and O. Vittori, Transfer of particles in nonisotropic air turbulence, J. Atmos. Sci. **32**, 565 (1975).
[5] J. Meyers and P. Sagaut, Is plane-channel flow a friendly case for the testing of large-eddy simulation subgrid-scale models? Phys. Fluids **19**, 048105 (2007).
[6] A. Rasam, G. Brethouwer, P. Schlatter, Q. Li, and A. V. Johansson, Effects of modelling, resolution and anisotropy of subgrid-scales on large eddy simulations of channel flow, J. Turbul. **12**, N10 (2011).
[7] D. R. Chapman, Computational aerodynamics development and outlook, AIAA J. **17**, 1293 (1979).
[8] H. Choi and P. Moin, Grid-point requirements for large eddy simulation: Chapman's estimates revisited, Phys. Fluids **24**, 011702 (2012).
[9] S. Chen, Z. Xia, S. Pei, J. Wang, Y. Yang, Z. Xiao, and Y. Shi, Reynolds-stress-constrained large-eddy simulation of wall-bounded turbulent flows, J. Fluid Mech. **703**, 1 (2012).
[10] A. Rouhi, U. Piomelli, and B. J. Geurts, Dynamic subfilter-scale stress model for large-eddy simulations, Phys. Rev. Fluids **1**, 044401 (2016).
[11] J. Jiménez and R. D. Moser, Large-eddy simulations: Where are we and what can we expect? AIAA J. **38**, 605 (2000).
[12] D. Chung and D. I. Pullin, Large-eddy simulation and wall modelling of turbulent channel flow, J. Fluid Mech. **631**, 281 (2009).
[13] J. Lee, M. Cho, and H. Choi, Large eddy simulations of turbulent channel and boundary layer flows at high Reynolds number with mean wall shear stress boundary condition, Phys. Fluids **25**, 110808 (2013).
[14] G. I. Park and P. Moin, An improved dynamic non-equilibrium wall-model for large eddy simulation, Phys. Fluids **26**, 015108 (2014).
[15] G. I. Park and P. Moin, Space-time characteristics of wall-pressure and wall shear-stress fluctuations in wall-modeled large eddy simulation, Phys. Rev. Fluids **1**, 024404 (2016).
[16] J. Deardorff, A numerical study of three-dimensional turbulent channel flow at large Reynolds numbers, J. Fluid Mech. **41**, 453 (2006).
[17] U. Piomelli, J. Ferziger, P. Moin, and J. Kim, New approximate boundary conditions for large eddy simulations of wall-bounded flows, Phys. Fluids A **1**, 1061 (1989).
[18] U. Schumann, Subgrid scale model for finite difference simulations of turbulent flows in plane channels and annuli, J. Comput. Phys. **18**, 376 (1975).
[19] E. Balaras, C. Benocci, and U. Piomelli, Two-layer approximate boundary conditions for large-eddy simulations, AIAA J. **34**, 1111 (1996).
[20] S. Kawai and J. Larsson, Wall-modeling in large eddy simulation: Length scales, grid resolution, and accuracy, Phys. Fluids **24**, 015105 (2012).
[21] W. H. Cabot and P. Moin, Approximate wall boundary conditions in the large-eddy simulation of high Reynolds number flow, Flow Turbul. Combust. **63**, 269 (2000).
[22] J. Larsson, S. Kawai, J. Bodart, and I. Bermejo-Moreno, Large eddy simulation with modeled wall-stress: Recent progress and future directions, Mech. Eng. Rev. **3**, 15 (2016).
[23] U. Piomelli and E. Balaras, Wall-layer models for large-eddy simulations, Annu. Rev. Fluid Mech. **34**, 349 (2002).
[24] S. T. Bose and G. I. Park, Wall-modeled large-eddy simulation for complex turbulent flows, Annu. Rev. Fluid Mech. **50**, 535 (2018).
[25] S. T. Bose and P. Moin, A dynamic slip boundary condition for wall-modeled large-eddy simulation, Phys. Fluids **26**, 015104 (2014).
[26] B. Perot and P. Moin, Shear-free turbulent boundary layers. Part 1. Physical insights into near-wall turbulence, J. Fluid Mech. **295**, 199 (2006).
[27] P. Orlandi, *Fluid Flow Phenomena: A Numerical Toolkit* (Springer, Berlin, 2000).

[28] J. Kim and P. Moin, Application of a fractional-step method to incompressible Navier-Stokes equations, J. Comput. Phys. **59**, 308 (1985).
[29] A. A. Wray, Minimal-storage time advancement schemes for spectral methods, NASA Ames Research Center report, 1990 (unpublished).
[30] M. Germano, U. Piomelli, P. Moin, and W. H. Cabot, A dynamic subgrid-scale eddy viscosity model, Phys. Fluids A **3**, 1760 (1991).
[31] D. K. Lilly, A proposed modification of the Germano subgrid-scale closure method, Phys. Fluids A **4**, 633 (1992).
[32] A. Lozano-Durán and J. Jiménez, Effect of the computational domain on direct simulations of turbulent channels up to $\mathrm{Re}_\tau = 4200$, Phys. Fluids **26**, 011702 (2014).
[33] H. J. Bae, A. Lozano-Durán, and P. Moin, Investigation of the slip boundary condition in wall-modeled LES, Stanford University Center for Turbulence Research Annual Research Briefs **2016**, 74 (2016).
[34] J. C. DelÁlamo, J. Jiménez, P. Zandonade, and R. D. Moser, Scaling of the energy spectra of turbulent channels, J. Fluid Mech. **500**, 135 (2004).
[35] S. Hoyas and J. Jiménez, Scaling of the velocity fluctuations in turbulent channels up to $\mathrm{Re}_\tau = 2003$, Phys. Fluids **18**, 011702 (2006).
[36] J. S. Baggett, On the feasibility of merging LES with RANS for the near-wall region of attached turbulent flows, Stanford University Center for Turbulence Research Annual Research Briefs **1998**, 267 (1998).
[37] J. Weatheritt, R. Sandberg, and A. Lozano-Durán, Reynolds stress structures in the hybrid RANS/LES of a planar channel, J. Phys.: Conf. Ser. **708**, 012008 (2016).
[38] J. Jiménez and A. Pinelli, The autonomous cycle of near-wall turbulence, J. Fluid Mech. **389**, 335 (1999).
[39] F. Waleffe, J. Kim, and J. M. Hamilton, *Turbulent Shear Flows 8* (Springer, Berlin, 1993), pp. 37–49.
[40] M. J. Walsh, Riblets as a viscous drag reduction technique, AIAA J. **21**, 485 (1983).
[41] P. J. Mason and D. J. Thomson, Stochastic backscatter in large-eddy simulations of boundary layers, J. Fluid Mech. **242**, 51 (2006).
[42] U. Piomelli, E. Balaras, H. Pasinato, K. D. Squires, and P. R. Spalart, The inner-outer layer interface in large-eddy simulations with wall-layer models, Int. J. Heat Fluid Flow **24**, 538 (2003).
[43] S. B. Pope, *Turbulent Flows* (Cambridge University Press, Cambridge, 2000).